Available online at www.sciencedirect.com
SCIENCE DIRECT
International Journal of Heat and Mass Transfer 49 (2006) 879–888
International Journal of HEAT and MASS TRANSFER
www.elsevier.com/locate/ijhmt

Molecular dynamics study of thin film instability and nanostructure formation

Minsub Han [a], Joon Sik Lee [a,*], Seungho Park [b], Young Ki Choi [c]

[a] School of Mechanical and Aerospace Engineering, Seoul National University, Seoul 151-742, Republic of Korea
[b] Department of Mechanical and System Design Engineering, Hongik University, Republic of Korea
[c] School of Mechanical Engineering, Chung-Ang University, Republic of Korea

Received 12 May 2004; received in revised form 24 August 2005
Available online 28 November 2005

Abstract

The instability dynamics of a thin liquid film at nanoscale on a substrate, which is confined by an upper wall at a distance, is studied by the molecular dynamics (MD) simulation. Two sources of instability are investigated in the context of nanostructure generation: (1) substrate heating; (2) electric field. In the case of instability induced by substrate heating, the temperature gradient in the film layer reaches up to 2.5 K per nanometer. A substantial amount of growth is observed at this temperature gradient for the waves with lower wave numbers. The thermocapillarity effect seems to be the major source of the instability. The electric field is imposed on the liquid film by considering the upper wall as an electrode. Three cases of different types of electrodes and interactions are compared on the instability characteristics. The electric field acts as a strong source of destabilization and consistently leads to the formation of structures bridging the substrate and the upper wall. In addition, present MD results are compared with those by the continuum theory, which shows a significant deviation from the present data in the prediction of the formation time.

1. Introduction

The instability of a thin liquid film has been studied extensively over the past 20 years [1]. The deformable surface of the film contains fluctuations that may grow in the significant amount under certain circumstances. They could lead to the breakup of the film or the meta-stable state. The phenomenon occurs in various contexts and contains rich dynamics in the process. It also has great significance in various fields of science and technology. For example, it plays a vital role in the industrial process like coating and drying or the function of biological systems like lung lining.

Recently, growing interest has been shown on the systems at nanoscale, one of which is on the field of nanostructure generation. There have been studies that the structures of the sub-microscale can be self-constructed by controlling the instability of thin fluid film [2,3]. A more recent study in regard to electrostatic nanolithography shows that similar phenomena can be realized with the atomic force microscopy [4]. They share the basic elements in the procedure. The thermoplastic polymer is usually used for the film material, and some heating and cooling processes are applied to induce the phase change. For example, embossed pattern or probe is used to induce the growth of waves on the film surface nearby. By controlling the measures, some intended pattern of the structure can be built up. And the methods have practical implications in the emerging small-scale technologies; the good examples are the electronic devices of the increasingly smaller dimension or the nano-electro-mechanical systems. It is then an important issue in implementing these methods to understand and predict the characteristics of the phenomena. For the design issues, as an example, it is required to better understand the pattern and formation time of the structures with respect to the set of materials and processes involved.

* Corresponding author. Tel.: +82 2 880 7117; fax: +82 2 883 0179.
E-mail address: jslee123@snu.ac.kr (J.S. Lee).

0017-9310/$ - see front matter © 2005 Elsevier Ltd. All rights reserved.
doi:10.1016/j.ijheatmasstransfer.2005.09.017

Nomenclature

A, $\bar{A}$, A_0, B	constants
$A(k,t)$	amplitude spectrum of wave number k
a	width of electrode strip
D	measure of density ratio ($=3\rho^{v}/2\rho$)
d	distance between the walls
d_0	mean film thickness
E	measure of evaporation effect ($=d_0\tilde{J}/\rho v$)
f	external force
G	Gibbs free energy
h	location of liquid–vapor interface
h_0	mean film thickness
h'	amplitude of fluctuation
J	evaporation rate
$\tilde{J}$	mean evaporation rate
k	wave number
k_s	spring constant
M	measure of thermocapillarity effect ($=\gamma d_0(\Delta T)_0/2\rho v^2$)
m	molecular mass
r	distance between atoms
S	measure of surface tension effect ($=\sigma d_0/3\rho v^2$)
s	growth rate
T	temperature
$(\Delta T)_0$	typical temperature difference between substrate and film surface
t	time
u	Van der Waals interaction energy
x, y, z	coordinates
z_0	distance from a point in the liquid film to the upper wall

Greek symbols

α	polarizability
β	fitting constant
γ	surface tension variation with respect to temperature ($=-\mathrm{d}\sigma_s/\mathrm{d}T$)
ε	energy parameter
λ	electric charge density
μ	permanent dipole moment
ν	kinematic viscosity
Ξ	electric field
ξ_f	permissivity of liquid medium
ξ_0	permissivity of free space
ρ	liquid density
ρ^{v}	vapor density
σ	intermolecular diameter
σ_s	surface tension
Φ	measure of external potential
ϕ	external potential
φ	electric potential

Subscripts

Ar	argon
h	derivative with respect to film thickness
max	maximum
Pt	platinum
t	time derivative
x	spatial derivative
z	component in the z direction

Several physical phenomena are involved in the methods. The heating processes may cause the evaporation or non-uniformity in the temperature field. In addition, as the ions or dipoles in the film may interact with the solid at a distance, their distribution may be distorted by the existence of the heated walls or electric field. The phenomena should be understood at nanoscales, but previous studies on the subject rely heavily on the continuum theory [5,6]. They include the molecular features in the model, such as the electrostatic and disjoining pressures, and use the long-wave approximation for the film evolution. These approaches seem to give reasonable predictions for the systems at the sub-microscale. However, it is debatable whether this approach is still valid for the phenomena at nanoscales. This is because non-continuum features may produce size effects on the dynamics. The inhomogeneity in the density and pressure may be a good example. Thus, a more realistic approach like the molecular dynamics (MD) simulation is necessary to enable reliable predictions for nanoscale structures.

The MD simulation seems a relevant approach for the present problem. The MD solves the equations of motion for the molecules directly, and requires little model other than the intermolecular potential [7]. Therefore, it is a powerful tool to probe a new phenomenon at nanoscale. In this study, the MD is used to investigate the dynamic behavior of the thin fluid film on a substrate during the destabilization and structure formation. As a first step to analyze various physical aspects of the problem, two sources of instability are considered: one is the heating process and the other is the application of electric field by electrode. The MD simulation is performed for each source, and the continuum theory is used to compare the results.

2. Methods

2.1. Theoretical background for the continuum model

The evolution equation can be obtained on the continuum basis for the thin liquid film on the substrate. The basic set of equations in the fluid dynamics is used with the assumptions that the film is of a homogeneous and Newtonian fluid and the wavelength of the disturbance is

sufficiently long [8]. The evolution equation of the film can be written as

$$h_t + EJ + S(h^3 h_{xxx})_x - \left[\left(\frac{E}{D}JJ_x + \Phi_x\right)h^3 + MT_h h^2 h_x\right]_x = 0, \tag{1}$$

where the dimensionless variables E, D, Φ, S, and M are defined as

$$E = \frac{d_0\tilde{J}}{\rho v}, \quad D = \frac{3}{2}\frac{\rho^{\mathrm{v}}}{\rho}, \quad \Phi = \frac{\phi d_0^2}{6\pi\rho v^2}, \quad S = \frac{\sigma_{\mathrm{s}} d_0}{3\rho v^2}, \quad M = \frac{\gamma d_0 (\Delta T)_0}{2\rho v^2}. \tag{2}$$

They represent the relative measures of the evaporation, density ratio, external potential, surface tension and Marangoni effect, respectively. h is the location of liquid–vapor interface and J is the evaporation rate. These two are scaled with respect to d_0 and $\tilde{J}$, which are the mean film thickness and mean evaporation rate, respectively. x is scaled by the typical wavelength. T_h is the temperature variation with respect to the film thickness at the interface and scaled by $(\Delta T)_0/d_0$, where $(\Delta T)_0$ is the typical amount of the temperature difference between the substrate and the film surface. ϕ is the external potential. σ_{s}, ρ, ρ^{v}, v are the surface tension, liquid and vapor densities, and kinematic viscosity, respectively. γ is defined as

$$\gamma = -\frac{\mathrm{d}\sigma_{\mathrm{s}}}{\mathrm{d}T}, \tag{3}$$

which is positive for common fluids. Note that the evaporation rate and temperature gradient are included explicitly in Eq. (1) like other properties.

As the thickness of the film approaches nanoscale, non-continuum characteristics becomes important. The microscopic feature like the electrostatic and disjoining pressures can be accounted for in the form of the external potential. Others left out in Eq. (1) may include the velocity and thermal slip on the solid surface, the inhomogeneity of density, and the stress caused by the thermal fluctuation in the liquid–vapor surface. The linear stability analysis then gives the following relationships. With

$$h = h_0 + h' \exp(\mathrm{i}kx + st), \tag{4}$$

the growth rate s for the wave of wave number k can be expressed as

$$s = -EJ_h + k^2\left[-\left(\frac{E}{D}J_h + \Phi_h + MT_h\right) - Sk^2\right]. \tag{5}$$

This indicates that the surface tension acts as a stabilizer. On the other hand, the negative gradient of the evaporation, potential and temperature with respect to the film thickness contribute to the destabilization of the film.

2.2. Simulation methods

Non-equilibrium molecular dynamics simulation [7,9] is conducted for a system which consists of argon atoms confined by two platinum walls as depicted in Fig. 1. Argon atoms interact with each other through 12–6 Lennerd-Jones (LJ) potential which is given by

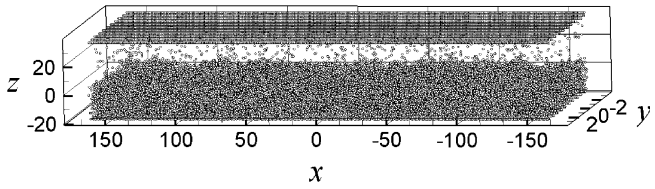

Fig. 1. A general view of the simulation domain, whose width can vary. The scales are normalized with respect to σ_{Ar}.

$$u(r) = 4\varepsilon\left[\left(\frac{\sigma}{r}\right)^{12} - \left(\frac{\sigma}{r}\right)^{6}\right], \tag{6}$$

where u is the interaction energy between two atoms that are separated by the distance r with the energy parameter ε and intermolecular diameter σ. For argon, $\varepsilon_{\mathrm{Ar}} = 1.67 \times 10^{-21}$ J and $\sigma_{\mathrm{Ar}} = 3.4 \times 10^{-10}$ m. The LJ interaction is cut off at $3\sigma_{\mathrm{Ar}}$. Each wall consists of three layers of platinum atoms [10,11]. Their equilibrium positions conform to the fcc lattice (1 1 1) with the distance between neighboring atoms of 2.77×10^{-10} m. The platinum atoms interact with each other through the harmonic potential with a spring constant $k_{\mathrm{s}} = 46.8$ N/m. The platinum walls are considered "insulated" in that the effect of free electron carrier is not included in the model. The temperature of the system is controlled by the "ghost" atoms located in the second row of the three layers of each wall [9]. They obey the Langevin equation whose parameters are adjusted to approximate the phonon characteristics of the semi-infinite solid phase [12]. The atoms in the outmost rows in the two walls are fixed in space. The platinum atom interacts with argon through LJ potential of $\varepsilon_{\mathrm{Ar-Pt}} = 1.009 \times 10^{-21}$ J and $\sigma_{\mathrm{Ar-Pt}} = 3.085 \times 10^{-10}$. With this value of $\varepsilon_{\mathrm{Ar-Pt}}$, the liquid argon wets the platinum wall [10]. The size of the computational domain is $W \times 2.4 \times 29.4$ nm^3, where the width, W, varies from 2.4 to 136 nm. The number of the simulated atoms varies accordingly from 3000 to 162,000. The depth in the y direction is chosen so that the smallest size possible is $7.06\sigma_{\mathrm{Ar}}$ to minimize the gradient in the direction as of the fluid experiment on the Hele-Shaw cell. The periodic boundary conditions are applied in all three directions. The Newton's equations of motion are integrated according to the velocity Verlet algorithm [9] with a time step of 5 fs ($=0.0025\varepsilon_{\mathrm{Ar}}^{1/2}/m_{\mathrm{Ar}}^{1/2}\sigma_{\mathrm{Ar}}$) is used. The liquid atoms are initially positioned in the fcc lattice close to the lower wall. The system is equilibrated for 0.1 ns (=20,000 steps) when a stable liquid film is formed on the lower wall.

3. Results and discussion

3.1. Instability by substrate heating

The first case to be considered is that the substrate temperature is increased from the initial state. As discussed

before, the substrate temperature is controlled by the atoms (ghost particles) embedded in the wall. The same target value of temperature is assigned on both of the walls even though the upper wall may not influence the liquid temperature significantly until the liquid comes into contact with it. A history of the temperature of ghost particles is chosen as shown in Fig. 2 such that it sustains a higher temperature gradient in the film layer. In Fig. 2, T_i is the initial temperature and the temperature oscillation from T_0 to T_1 is imposed on the ghost particles. It is stressed that the target temperature value of the ghost particles is not that of the wall layer in contact with liquid. By a number of tries, it is found that a constant temperature condition for the ghost particles does not produce a higher temperature gradient in the liquid film over a given simulation time. On the other hand, a constant heat-flux condition would soon increase the temperature at the wall–liquid interface to the evaporation point, and make the whole film depart from the wall. The drastic oscillatory nature of the assigned values for the ghost particles in the initial history in Fig. 2 does not make the film temperature oscillate in the same way partly because the thermal resistance at the interface and the thermal diffusion of liquid may dampen the effects. The oscillatory values help the high temperature gradient be sustained initially. This history may not produce the maximum possible or unique one, the search for which is not the main purpose of this study. Even with the drastic and oscillatory nature of the assigned values for the ghost particles, the film maintains the temperature gradient of about 2.5 K per nanometer in a relatively constant manner after the initial period of equilibration as illustrated in Fig. 3. Fig. 3 shows temperature variation between the walls with time. It can clearly be seen that the temperature remains practically constant in the liquid layer, which occupies the region up to about $z = 2$.

To analyze the film evolution, it is necessary to keep track of the location of the liquid–vapor interface. At the atomic scale, the interface is of a diffuse and finite region. This requires some adequate definition about the interface location. The first candidate would be the Gibbs dividing surface, that is, a surface which divides the interfacial

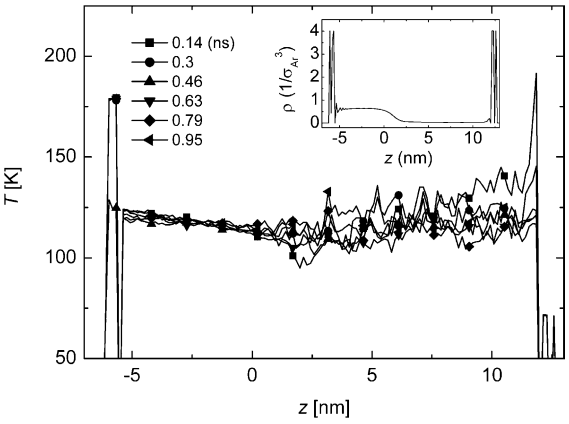

Fig. 3. Typical temperature profiles and density variation during substrate heating. The temperatures are averaged over 50 ps. The data in the vapor phase are more scattered because of the limited sample numbers in the region. The density is averaged over the whole simulation time.

region to take into account of density variation from the liquid to vapor in the finite region in such a way that the resultant total mass should be the same as that of the finite interfacial region. In the cases considered here, the interface evolves with time in the arbitrary shape, which may make this precise measurement rather cumbersome. In this study, the density distributions are averaged over a time period of 13.5 ps. The interface is followed by tracking the location of the density of a median value. The snapshots of the film evolution reveal that the film surface contains large amount of fluctuations at various scales. The capillary waves in addition to the thermal fluctuation are always present. The wave growth at a relatively early stage had better be identified through a spectral analysis.

The amplitude spectral density (ASD) can be obtained by

$$|A(k,t)| = \left| \int \mathrm{d}x \exp(-\mathrm{i}kx) h(x,t) \right|. \tag{7}$$

The typical result is shown in Fig. 4. The width of the simulation domain is about 54 nm and, therefore, any wave of a wavelength longer than this is suppressed by the periodic boundary condition. Initially, the waves are distributed

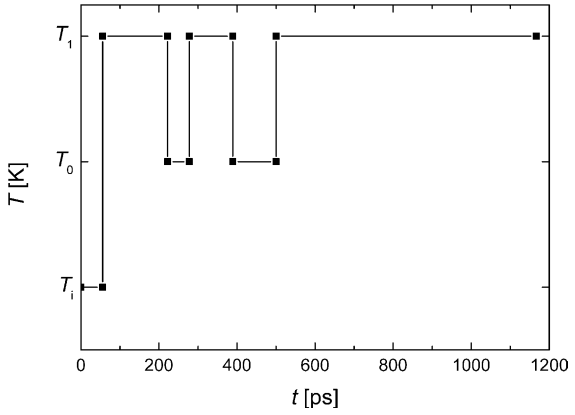

Fig. 2. History of the assigned temperature for ghost particles.

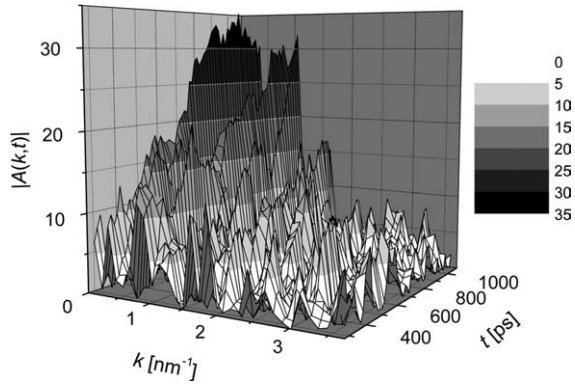

Fig. 4. The amplitude spectra of $T_i = 72$ K, $T_0 = 120$ K, and $T_1 = 180$ K.

over the large span of wave number in a random fashion. As they evolve, the ASD of a few of them grow consistently while those of others either grow initially but die out quickly afterwards or simply fluctuate at a certain level. The increases in the ASD of these wave numbers are due mainly to their growth rather than the decay of the waves of other wave numbers, and growing waves are in the region of lower wave number values. The wave of the highest ASD ($k = 0.35\ \mathrm{nm}^{-1}$) is of the wavelength with one-third of the maximum. Even the wave of the highest ASD does not grow indefinitely but stagnates at some point. This can be shown more clearly in Fig. 5, where the ASD of the highest growing waves for different thermal histories are plotted. T_1 in Fig. 2 varies from 54 to 180 K. They all grow for some time to varying degrees but stagnate in the given time. More data for other thermal histories are omitted for the clarity of view but follow similar trends.

The source of the instability may be identified with the help of the analysis based on the continuum theory. The effect of evaporation over the surface tension, $-(EJ_h/D)/S$ (see Eq. (5)), is not of an appreciable amount in the cases considered except for the very initial stage. The position of the liquid–vapor interface is tracked down by calculating the density profile and by following the positions of the median density value between those of the bulk liquid and vapor. The evaporative mass flux can be estimated by subtracting the mass flux due to the interfacial movement from the total mass flux at the interface. No appreciable gradient with respect to the height, J_h, is observed.

The effect of the thermocapillarity over the surface tension, $-MT_h/S$, for different thermal histories considered in Fig. 5, is illustrated in Fig. 6. The surface tension with respect to temperature variation is measured in the equilibrium state by the standard methods in which the difference in the pressure tensor in the normal and tangential directions is integrated over the interfacial region. From the temperature profile averaged over the width, $-MT_h/S$ is obtained for each time period of 12.5 ps during the evolution. The raw data is quite scattered that they are smoothed with 5 adjacent points with minimal deviation from overall trends. In Figs. 5 and 6, it may be suggested that, with a higher value of $-MT_h/S$, the growth sustains for a longer period. Therefore, the thermocapillary effect may play a large part in the instability, and growth of a longer period may require a system that maintains a higher value of $-MT_h/S$.

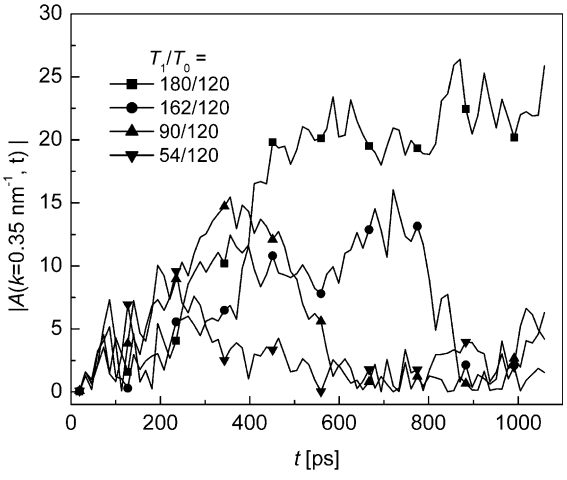

Fig. 5. Evolution of ASD at $k = 0.35\ \mathrm{nm}^{-1}$ for various temperature histories.

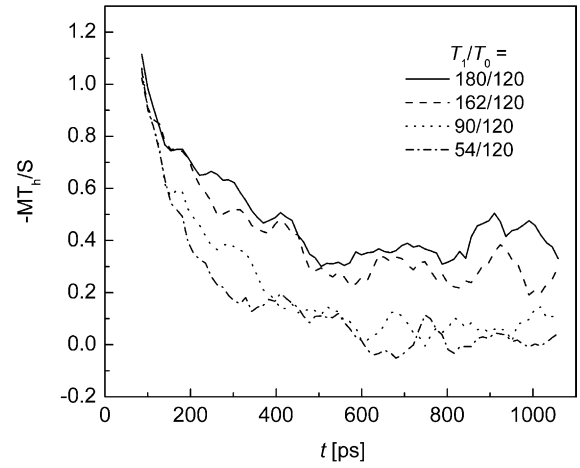

Fig. 6. The measure of the thermocapillary effect over surface tension, $-MT_h/S$, obtained from the measurements for each time period of 12.5 ps. The data are smoothed with adjacent 5 points.

3.2. Instability by the electric field

With substrate heating, the growth of instability is not so sufficient that the vertex of the wave does not reach the upper wall. For example, even in the case with a width of 166.2 nm, which is the longest one considered, the waves do not grow enough to form a vertical structure bridging the two walls.

Another source of instability is thus considered in the context of the structure formation. It is the long-range attraction by the upper wall. In the film evolution shown in the previous cases, the wave does not grow enough to reach the active region of intermolecular potential of the upper wall. This is mainly because the Van der Waals interaction between the fluid and solid atoms is of a relatively short-ranged one when compared to the distance between the film surface and the upper wall. The interaction is cut off at the distance of $3\sigma_{\mathrm{Ar}}$ in the simulation, where its strength decays to a value less than 0.6% of the well depth of the potential. Among those that decay slower are the ones involving ion or dipole. When the attractive force imposed on the liquid by the upper wall cannot be negligible, it can be a natural source of destabilization against the stabilizing surface tension. The phenomena are investigated with the system augmented with a simple potential.

A thin fluid film on the substrate is considered at a distance from the electrode. If the film is composed of ions or dipoles, it interacts with the electric field of the electrode.

Even when the fluid consists solely of non-polar molecules, the electric field may produce induced dipoles on them that interact with it. Based on these interactions, the liquid film near the electrode may effectively be under some external forces. The interactions are of longer-ranged ones than that of Van der Waals. In general, the calculation of the long-range interactions requires a special treatment for their slowly-decaying part because simple truncation may lead to divergent error. Several algorithms are developed for the problem but are still computationally demanding for the simulation of waves even at a modest size [9]. Instead, a simpler approach is available if we focus on the characteristics of thin film evolution while adopting some approximations that still keep the basic physical elements of the problem. It is here assumed that the atoms in the film are subject to a *stationary* electric field during the entire evolution. This may neglect the dynamic effect of the electric field caused by the surrounding atoms, that is, another ions, dipoles, or induced dipoles. The responses of the electron distribution in the electrode to the film evolution can also be neglected. For example, the redistribution of the charge in the electrode or the strong ordering of the permanent dipole in the film may take place as the film gets closer to the electrode. The former contribution can be compensated by using some effective models for the interactions. One of them is to use the permissivity of the liquid medium in place of that of free space, which alters only the overall strength of the interaction. The justification for the latter contribution is that the major characteristics of the film evolution are determined in the initial stage when the film is still located some distance away from the electrode. More rigorous study may then be required when the focus is more on the liquid evolution close to the electrode.

Based on these considerations, three kinds of physical systems are studied as depicted in Fig. 7. In Case I, the liquid film of point dipoles is at some distance from a line charge. Case II is that of non-polar atoms near the line charge. Finally, Case III deals with the film of non-polar atoms near the electrode of an infinite strip. The first system is the simplest one and thus studied in more details. Its result is then qualitatively compared with those of other systems.

The electric field in the distance of z from an infinite line charge whose axis is in the x direction is given by

$$\Xi_z = \frac{1}{4\pi\xi_0}\frac{2\lambda}{z}. \tag{8}$$

Accordingly, a dipole in the distance of z from the line charge is under the external force in the amount of

$$f_z = \frac{1}{4\pi\xi_0}\frac{2\mu_z\lambda}{z^2}. \tag{9}$$

The direction of the force is either away from or towards the electrode depending on the sign of the charge. The permanent dipoles in the liquid are randomly oriented due to thermal fluctuation in the absence of the external field such that the average value, $\bar{\mu}_z$, is zero. However, the presence of the electric field induces ordering of the dipole moment whose average value is not negligible and depends on the temperature as well as the field strength. As is discussed before, the dipole moment of the point dipole is assumed to be sufficiently weak so that the average dipole moment and the permissivity in the film depend weakly on the distance, and are assumed to be constants. Again the emphasis is on the dynamic evolution of the film subject to some external forces rather than rigorous modeling of the given physical system. The liquid film is then under the external force of

$$f_z = \frac{\bar{A}}{z^2}, \tag{10}$$

where

$$\bar{A} = \frac{\bar{\mu}_z\lambda}{2\pi\xi_f}. \tag{11}$$

The system for the molecular dynamics simulation is similar as in Section 3.1 except for the application of the external force on each atom. The electrode is located on the first row of the solid lattice in the upper wall (see Fig. 7, Case I). The solid atoms in the upper wall interact

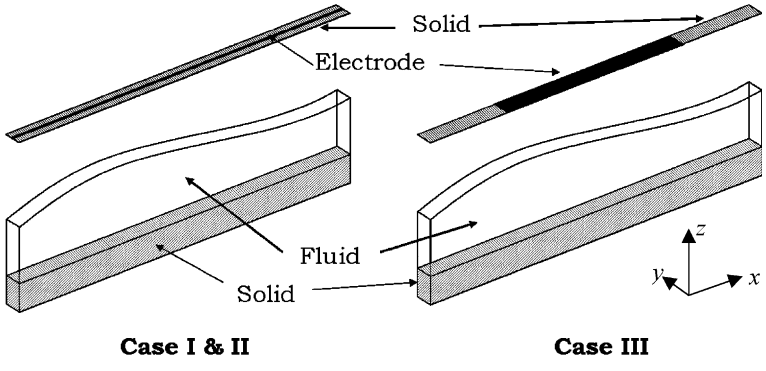

Fig. 7. The schematic of simulation systems. In Case I and II, a line charge is located on the upper wall and the perfect slip condition is applied on the surface normal to y. In Case III, an electrode of an infinite strip is located. The periodic conditions are applied in all directions.

with liquid atoms only repulsively. The attractive force on an atom at a distance of $z_0\sigma$ from the solid surface is then given by

$$f_z = \frac{A}{z_0^2}, \tag{12}$$

where

$$A = \frac{\bar{\mu}_z \lambda}{2\pi \xi_f \varepsilon \sigma}. \tag{13}$$

The slip boundary condition is applied on the boundaries normal to the y axis and the periodic condition is applied on those normal to other axes. The typical size of the problem considered is of $110.8 \times 29.4 \times 2.4\ \mathrm{nm}^3$. During the equilibration period of 0.11 ns, the solid potential is not applied. In most cases, the simulations last up to 1.46 ns. The temperature of the ghost particles in the walls is set as 108 K and no other measure is taken to control that of the fluid film. The rest of the details on the simulations are the same as the case in Section 3.1. The values of A in the range of 3.5–17 are simulated. The unit value of A corresponds to $\bar{\mu}_z \lambda$ of $3.1348 \times 10^{-41}\ \mathrm{C}^2$ with the material parameters of argon. The film becomes unstable enough to form vertical structures consistently as shown in Fig. 8.

All the results follow the trends that the time for the formations gets shorter as the strength of the solid potential gets stronger as can be seen in Fig. 9. The formation time is obtained from the snapshots measured at every 10.8 ps. The moment of formation is chosen when the wave crest grows enough to make contact with the upper wall and the contact angle is formed. The circle symbols indicate the formation time, which are fitted with the relationship of $\Delta t \sim A^{\beta}$. Δt is the formation time period, and β is found to be -1.179 with the SD of 0.1556. The time is also measured when the amplitude of the wave reaches 25% of the initial film thickness. The film density is averaged over the time period of 10.8 ps, and the moment is chosen when the position in the interfacial region where the density is a half of the bulk value reaches 25% of the initial film thickness. The data denoted by square symbols show the trend similar to the formation time with $\beta = -1.205$ and the deviation of 0.1813. The number of the vertical structures increases from 1 to 4 with the strength of the electric field, A.

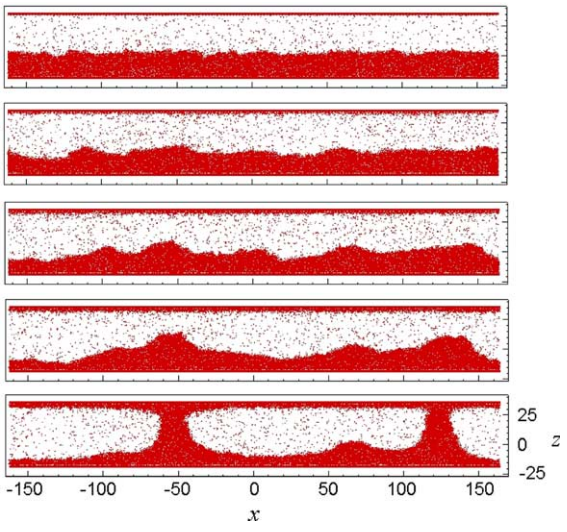

Fig. 8. The snapshots of the film evolution and vertical structure formation in the presence of the attracting solid wall at $A = 7.8$. Each instance is taken at 0, 216.1, 432.2, 648.3, and 864.4 ps, respectively.

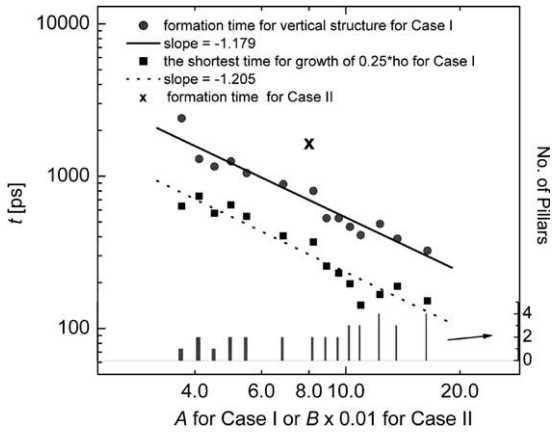

Fig. 9. The time periods for the first vertical structure formation: circle and cross. The error for the measurement is about ±10.8 ps. The time periods of the growth up to 25% of the initial film thickness for the fastest-growing disturbance: square. It is based on the density profile data averaged over 10.8 ps. The SDs for the solid line and dotted lines are 0.1556 and 0.1813, respectively.

The simulation results are compared with those of the continuum theory. The expression for the external potential or disjoining pressure in Eq. (5) due to the electric field can be derived by following the steps suggested by Derjaguin [13]. The increase in the free energy per unit area by the existence of the upper wall can be obtained by integrating the solid potential over the film thickness. It follows that

$$G(d) = \int_0^h \sigma^3 \rho \left(-\frac{A}{d-z} \right) \mathrm{d}z = A\sigma^3 \rho \ln \frac{d-h}{d}, \tag{14}$$

where d is the distance between the walls. All properties are non-dimensionalized except for ρ and σ. The disjoining pressure is obtained by taking the derivative of it with respect to d as follows:

$$\Phi = -\left. \frac{\partial G}{\partial d} \right|_{h,T} = -A\sigma^3 \rho \frac{h}{d(d-h)}. \tag{15}$$

Then, it follows that

$$\Phi_h|_{d=\text{constant}} = -\frac{A_0}{(d-h)^2}, \tag{16}$$

where A_0 is given by

$$A_0 = \sigma^3 \rho A. \tag{17}$$

When this is put into Eq. (5), the instability criterion can be determined. As is considered before, this may induce the instability when Φ_h is of a negative value. From Eqs. (4) and (5), the maximum growth rate $s_{\max}$ can be expressed as

$$s_{\max} = \frac{A_0^2}{4S(d-h)^4} \tag{18}$$

and for the wave number $k_{\max}$,

$$k_{\max}^2 = \frac{A_0}{2S(d-h)^2}. \tag{19}$$

Since

$$h_{\max} \sim \exp(A_0^2 t) \sim \exp(A^2 t), \tag{20}$$

the continuum theory predicts that the time for the maximum film growth should be

$$\Delta t \sim A^{-2}. \tag{21}$$

Therefore, the continuum theory overpredicts the decreasing rate of the growth time with respect to the strength of the potential when compared with the MD simulation results. This is not due to the domain size because, as the numbers of the vertical structures formed suggest, the simulation domain is large enough to contain the maximum growing wave.

First, the dependence of the disjoining pressure is checked with respect to the potential strength. Fig. 10 shows the normal pressure of the film in equilibrium, which is measured with respect to the strength of the solid potential. It is equivalent to the disjoining pressure in the film [14]. In each measurement, the film is equilibrated over 0.27 ns and the pressure tensor values are collected over 2.16 ns. The temperature is set as 108 K. The molecular velocities are rescaled at every 54 ps to minimize the temperature drift. As the potential gets stronger, it becomes difficult to keep the film stable during the measurements. The atoms in the vapor phase at a distance longer than $10\sigma_{Ar}$ from the film surface are free from the influence of the potential, which makes the film more stable. Even with this measure, it is not possible to get the data for the cases of $A > 10.9470$. The results show that the disjoining pressure has a linear dependence on the strength of the electric field as in the continuum theory given by Eq. (15). Therefore, it may not be the source of the discrepancy.

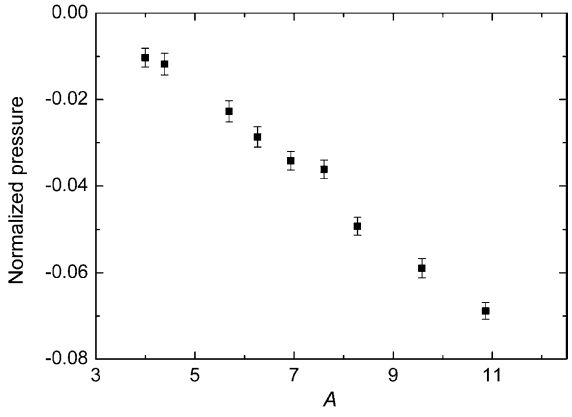

Fig. 10. The pressures normal to the film surface. The measurements are done over 2.16 ns.

The adequacy in other approximations in the continuum theory is considered. The ratios of the mean thickness of the film to the wavelength of the fastest-growing fluctuation vary from about 0.063 to 0.25. For the data set fitted by the dotted line in Fig. 9, the ratios of the amplitude to the wavelength of the fastest-growing one vary from about 0.016 to 0.063. If the usual criterion for the long wave is less than about 0.1, the approximation does not cause the problem.

The change in the properties like density, viscosity, and surface tension may play some role. The very strong potential and thereby evolution in a very short time may contribute to the discrepancy. It may also be questioned if the theory for the disjoining pressure in the dynamics of the thin film is still valid at the molecular scale. To resolve the issue, it seems necessary to examine the process of film evolution closely with more quantitative comparisons.

The second system in consideration is the film of non-polar atoms in some distance from a line charge. The line charge exerts an attractive force on a non-polar atom in the amount of

$$f(r) = \frac{B}{z^3}, \tag{22}$$

where

$$B = \frac{4\alpha\lambda^2}{\varepsilon\sigma^2}. \tag{23}$$

This interaction can be compared with the previous case in two aspects. It depends on the inverse third power of the distance, which is shorter-ranged one than that of Case I, and is also proportional to the polarizability. Because of these two features, the interaction becomes less effective in inducing the instability. This is indicated as a cross symbol in Fig. 9. The same simulation system is used with the external force given by Eq. (10). The data point is for the case of two-pillar formation and the charge density of $\lambda = 4.56 \times 10^{-7}$ C/m with argon parameters.

Finally, while the semi-infinite electrode does not exert any force on the dipole or non-polar atom, the electrode of an infinite strip does because it applies a non-uniform electric field. If we consider the case of an infinite strip with a width a, its electric potential φ satisfies

$$\frac{x^2}{(a\cosh\varphi)^2} + \frac{z^2}{(a\sinh\varphi)^2} = 1. \tag{24}$$

The electric field is then given by

$$\vec{\Xi} = \left(-\frac{\lambda}{2\pi\xi_0}\frac{\partial\varphi}{\partial x}, -\frac{\lambda}{2\pi\xi_0}\frac{\partial\varphi}{\partial z}\right). \tag{25}$$

Then, the electrode applies the force on a non-polar atom nearby in the amount of

$$\vec{f} = \alpha\vec{\Xi}\cdot\nabla\vec{\Xi} = \alpha\left(\frac{\lambda}{2\pi\xi_0}\right)^2\left(\frac{\partial\varphi}{\partial x}\frac{\partial^2\varphi}{\partial x^2} + \frac{\partial\varphi}{\partial y}\frac{\partial^2\varphi}{\partial y\partial x}, \frac{\partial\varphi}{\partial x}\frac{\partial^2\varphi}{\partial x\partial y} + \frac{\partial\varphi}{\partial y}\frac{\partial^2\varphi}{\partial y^2}\right). \tag{26}$$

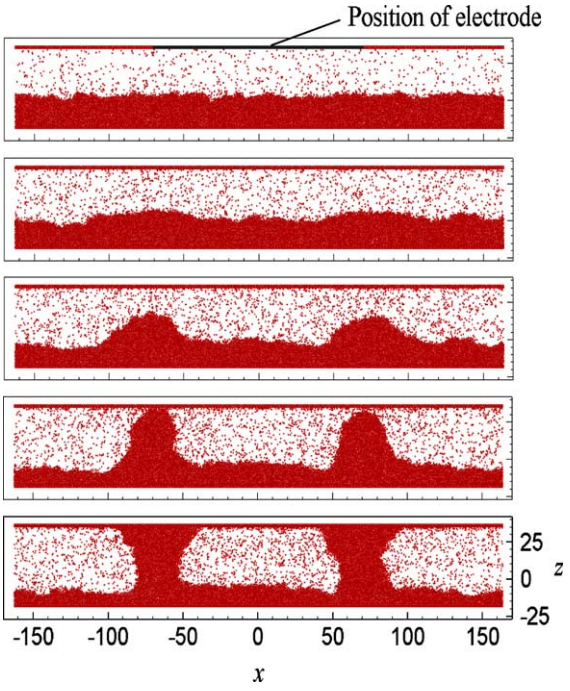

Fig. 11. The snapshots of the film evolution subject to an electrode strip. Each snapshot is taken at 0, 100, 200, 300, and 400 ps, respectively.

In Fig. 11, the electrode of the infinite strip is located at the first row of the fcc lattice of the upper wall. The strip is 162.94σ in width, which is a half of the domain size in x, and located at the center in x. All the simulation conditions are the same as Case I and II except that the periodic boundary conditions are applied on all boundaries. The case shown in Fig. 11 corresponds to $\lambda = 6.5080 \times 10^{-2}\,\mathrm{C/m^2}$ for argon. The film surface becomes unstable at two positions simultaneously and pillars are formed there. The positions roughly coincide with those of the edges of the electrode. As is indicated in the equi-potential lines according to Eq. (24), the electric field is the strongest near the edges. The relatively large value of the charge density indicates that the film is more resistant to instability than those of the previous two cases.

4. Summary

The instability dynamics of a thin liquid film at nanoscale has been investigated by MD simulations. We consider the processes that destabilize the film on the solid substrate, and induce the vertical structures formed between the substrate and the upper wall, which have a practical significance in generating nanostructures. As a first step to analyze various physical aspects of the problem, two sources of instability are considered: the heating process and the attractive potential of the wall at a distance.

Firstly, a steep temperature gradient up to 2.5 K per nanometer is realized by controlling the temperature of the walls. Large fluctuations of various length scales at the film surface are observed, which are inherent in the molecular scale due to the capillary waves as well as the random thermal motions of atoms. Among them, a substantial amount of growth in the heating process occurs for the waves with lower wave numbers. The effect of thermocapillarity is appeared to be the major source of the instability, which is consistent with the continuum theory.

Secondly, we study the evolution of the film under the electric field by electrodes at a distance. Three different kinds of cases are considered. The first one is that a slab of liquid with a permanent dipole is located near the electrode of a line charge. The second one is on the liquid of induced dipole in the previous system. The last one is on the liquid of induced dipole near the electrode of an infinite strip. It is shown that a finite amount of attraction in the distance normal to the surface by the electric field is a strong source of destabilization. The fluctuations grow enough to reach the wall in the distance and consistently build up structures bridging the two walls. In the first case, it is observed that the formation time and the space between the structures is getting shorter as the relative strength of the electric field becomes larger. While this fact is consistent qualitatively with the continuum theory, the quantitative prediction of the theory deviates quite significantly from the MD simulation results. The continuum theory predicts that the formation time is proportional to the relative strength of the potential to the exponent of -2, which deviates from the MD results about a factor of two. This results from the nano-fluidic behaviors that are not accounted for in the continuum theory.

Acknowledgement

The authors gratefully acknowledge that this work is supported by Micro Thermal System Research Center through the SRC/ERC program of MOST/KOSEF.

References

[1] A. Oron, S.H. Davis, S.G. Bankoff, Long-scale evolution of thin liquid films, Rev. Mod. Phys. 69 (1997) 931–980.
[2] S.Y. Chou, L. Zhuang, Lithographically induced self-assembly of periodic polymer micropillar arrays, J. Vacuum Sci. Technol. B 17 (6) (1999) 197–3202.
[3] E. Schaffer, T. Thurn-Albrecht, T.P. Russell, U. Steiner, Electrically induced structure formation and pattern transfer, Nature 403 (2000) 874–877.
[4] S.F. Lyuksyutov, R.A. Vaia, P.B. Paramonovi, S. Juhl, L. Waterhouse, R.M. Ralich, G. Sigalov, E. Sancaktar, Electrostatic nanolithography in polymers using atomic force microscopy, Nat. Mater. 2 (2003) 469–472.
[5] L. Wu, S.Y. Chou, Dynamic modeling and scaling of nanostructure formation in the lithographically induced self-assembly and self-construction, Appl. Phys. Lett. 82 (19) (2003) 3200–3202.
[6] S. Herminghaus, Dynamical instability of thin liquid films between conducting media, Phys. Rev. Lett. 83 (12) (1999) 2359–2361.
[7] D.C. Rapaport, The Art of Molecular Dynamics Simulation, first ed., Cambridge University Press, Cambridge, 1995.

[8] J.P. Burelbach, S.G. Bankoff, S.H. Davis, Nonlinear stability of evaporating/condensing liquid films, J. Fluid Mech. 195 (1988) 463–494.
[9] M.P. Allen, D.J. Tildesley, Computer Simulation of Liquids, first ed., Oxford University Press, New York, 1987.
[10] S. Maruyama, T. Kimura, A molecular dynamics simulation of a bubble nucleation on solid surface, Int. J. Heat Technol. 18 (Suppl. 1) (2000) 69.
[11] P. Yi, D. Poulikakos, J. Walther, G. Yadigaroglu, Molecular dynamics simulation of vaporization of an ultra-thin liquid argon layer on a surface, Int. J. Heat Mass Transfer 45 (2002) 2087–2100.
[12] J.C. Tully, Dynamics of gas–surface interactions: 3D generalized Langevin model applied to fcc and bcc surfaces, J. Chem. Phys. 73–74 (1980) 1975–1985.
[13] B.V. Derjaguin, Theory of Stability of Colloids and Thin Films, Consultants Bureau, New York, 1989, pp. 23–31.
[14] D. Bhatt, J. Newman, C.J. Radke, Molecular simulation of disjoining-pressure isotherms for free liquid, Lennard-Jones thin films, J. Phys. Chem. B 106 (2002) 6529–6537.